Article:

Sartor, P., Becker, W., Worden, K. orcid.org/0000-0002-1035-238X et al. (2 more authors) (2016) Bayesian Sensitivity Analysis of Flight Parameters in a Hard-Landing Analysis Process. Journal of Aircraft, 53 (5). pp. 1317-1331. ISSN 0021-8669

https://doi.org/10.2514/1.C032757

Bayesian Sensitivity Analysis of Flight Parameters in a Hard Landing Analysis Process

Journal:	*Journal of Aircraft*
Manuscript ID	2013-12-C032757.R2
Manuscript Type:	Full Paper
Date Submitted by the Author:	n/a
Complete List of Authors:	Sartor, Pia; University of Bristol, Department of Aerospace Engineering Becker, William; European Commission, Joint Research Centre Worden, Keith; University of Sheffield, Department of Mechanical Engineerin Schmidt, R.; Messier-Bugatti-Dowty, A350 Programme Chief Engineer Bond, David; Messier-Bugatti-Dowty, Vice President Engineering
Subject Index Category:	01700 Landing Dynamics < 00000 AIRCRAFT TECHNOLOGY, CONVENTIONAL, STOL/VTOL, 02800 Simulation < 00000 AIRCRAFT TECHNOLOGY, CONVENTIONAL, STOL/VTOL

Note: The following files were submitted by the author along with the article. You may review these files online, if you wish. Acceptance for publication will be based solely on the content of the article.

AIAA_Latex_files_Pia_Sartor18 November 2015.7z

Bayesian Sensitivity Analysis of Flight Parameters in a Hard Landing Analysis Process

Pia Sartor[1]
Department of Aerospace Engineering, University of Bristol,
Queens Building, University Walk, Bristol,
BS8 1TR, UK, Email: pia.sartor@bristol.ac.uk

William Becker[2]
Econometrics and Applied Statistics, European Commission
- Joint Research Centre, TP 361, 21027 Ispra, Italy

Keith Worden[3]
Department of Mechanical Engineering,
University of Sheffield, Mappin Street, Sheffield, S1 3JD, UK

R. Kyle Schmidt[4] and David Bond[5]
Messier-Bugatti-Dowty, Cheltenham Road East, Gloucester, GL2 9QH, UK

A Flight Parameter Sensor Simulation (FPSS) model was developed to assess the conservatism of the landing gear component loads calculated using a typical hard landing analysis process. Conservatism exists due to factors of safety that are incorporated into any hard landing analysis process to account for uncertainty in the measurement of certain flight parameters. The FPSS model consists of: (1) an aircraft and landing gear dynamic model to determine the 'actual' landing gear loads during a hard landing; (2) an aircraft sensor and data acquisition model to represent the aircraft sensors and flight data recorder systems to investigate the effect of signal processing on

[1] Lecturer
[2] Postdoctorial Researcher
[3] Professor
[4] Programme Chief Engineer
[5] Vice President Engineering

the flight parameters; (3) an automated hard landing analysis process, representative of that used by airframe and equipment manufacturers, to determine the 'simulated' landing gear loads. Using a technique of Bayesian sensitivity analysis, a number of flight parameters are varied in the FPSS model to gain an understanding of the sensitivity of the difference between 'actual' and 'simulated' loads to the individual flight parameters in symmetric and asymmetric, two-point landings. This study shows that the error can be reduced by learning the true value of the following flight parameters: longitudinal tire-runway friction coefficient, aircraft vertical acceleration (related to vertical descent velocity), lateral acceleration (related to lateral velocity), Euler roll angle, mass, centre of gravity position and main landing gear tire type. It was also shown that due to the modelling techniques used, shock absorber servicing state and tire pressure do not contribute significantly to the error.

Nomenclature

CG	=	Aircraft Centre of Gravity
CS	=	Certification Specification
DOE	=	Design of Experiments
FAR	=	Federal Aviation Regulations
$FDIU$	=	Flight Data Interface Unit
FDR	=	Flight Data Recorder
$FPSS$	=	Flight Parameter Sensor Simulation
$GEM\text{-}SA$	=	Gaussian Emulation Machine for Sensitivity Analysis
GP	=	Gaussian Process
$mass$	=	Aircraft mass
MEI	=	Main Effects Index
MLG	=	Main Landing Gear
MSE	=	Normalised Mean Square Error
$Port\ SA$	=	Port main landing gear servicing state
$Starboard\ SA$	=	Starboard main landing gear servicing state
TEI	=	Total Effects Index
$tire$	=	Tire type
$tire\ press$	=	Tire pressure
V_{A_x}	=	Aircraft longitudinal velocity
V_{A_y}	=	Aircraft lateral velocity
V_{A_z}	=	Aircraft vertical descent velocity
$VRTG$	=	Aircraft vertical acceleration
$LATG$	=	Aircraft lateral acceleration
F_{actual}	=	'Actual' landing gear output data
$F_{simulated}$	=	'Simulated' landing gear output data
θ	=	Aircraft Euler pitch angle
ϕ	=	Aircraft Euler roll angle
ψ	=	Aircraft Euler yaw angle

μ_{long}	=	Longitudinal tire-runway friction coefficient
μ_{lat}	=	Lateral tire-runway friction coefficient
$\sigma^2_{F_{actual}}$	=	Variance of the 'actual' landing gear output data
$\sigma^2_{F_{simulated}}$	=	Variance of the 'simulated' landing gear output data
B	=	Roughness coefficients for the GP covariance function
$c(\cdot,\cdot)$	=	Covariance function of the GP
$c^*(\cdot,\cdot)$	=	Posterior covariance function of the GP
d	=	Number of model input parameters
cov	=	Covariance
$E(\cdot)$	=	Expected value
$h(\cdot)$	=	Regression function of the GP
$m(\cdot)$	=	Mean function
$m^*(\cdot)$	=	Posterior mean function
n	=	Number of training data points
$p(\cdot)$	=	Multivariate probability distribution
σ^2	=	Scaling factor of the GP covariance function
S_i	=	Scaled main effect index of input x_i
S_{Ti}	=	Scaled total effect index of input x_i
$t(\boldsymbol{x})$	=	Covariance of $\mathbf{x}$ with all training data
V_i	=	Unscaled main effect index of input x_i
V_{Ti}	=	Unscaled total effect index of input x_i
var	=	Variance
$\mathbf{w}$	=	Regression function coefficients
$\mathbf{x}$	=	Model input
$\mathbf{X}$	=	Uncertain model input
y	=	Model output
$\mathbf{Y}$	=	Uncertain model output
$z(x_i)$	=	Main effect
$z(x_{i,j})$	=	First order interaction

I. Introduction

A static structural overload occurs when a landing gear exceeds its material yield point in any location. A common aircraft operational occurrence which may result in a landing gear overload is a hard landing. A hard landing is defined by the regulatory authorities in EASA Certification Specification (CS) 25 and Federal Aviation Regulations (FAR) 25 as a landing with a limit vertical descent velocity exceeding 10 ft/s at the design landing weight [1, 2]. However, the effect of the vertical descent velocity must be combined with other critical enveloping flight parameters, including: aircraft gross weight, aircraft centre of gravity location, aircraft orientation (pitch, roll, yaw), rates of motion (pitch rate, roll rate, yaw rate), ground speed, vertical descent velocity, longitudinal, lateral and vertical acceleration, shock absorber servicing state and the tire-runway friction coefficient, to accurately assess the loads in the landing gear.

If the flight crew suspect that there has been a hard landing, the following analysis process is typically performed: (i) the flight crew makes an occurrence declaration; (ii) visual and Non-Destructive Testing (NDT) inspections are performed on the landing gear by the operator's maintenance crew to assess for damage to the landing gear and airframe structure; (iii) aircraft flight parameter data, such as aircraft acceleration, ground speed and aircraft orientation (pitch, roll), are downloaded from the Flight Data Recorder (FDR) and reported to the aircraft and landing gear manufacturers, who then calculate the loads during the occurrence [3]. Only after the data have been analyzed can it be determined if there has been an overload.

A degree of conservatism typically exists in current hard landing analysis processes to ensure safety of aircraft operation. This conservatism evolves from factors of safety or conservative assumptions included within the analysis process to account for: (i) uncertainty in measured aircraft flight parameters and (ii) unavailable aircraft flight parameters. For example, on common short and medium range aircraft, vertical acceleration is typically sampled at 8 Hz. A landing however, takes less than 125 ms. Thus, a possibility exists that the peak vertical acceleration recorded on the FDR is less than the actual maximum value. To date, the effect of such assumptions on the degree of conservatism in a hard landing analysis process has not been quantified [4].

A Flight Parameter Sensor Simulation (FPSS) model has been developed to assess the conservatism in a hard landing analysis process [5]. Using a technique of Bayesian sensitivity analysis, a number of flight parameters are varied in the FPSS model to gain an understanding of how the model responds to variations in the inputs, to identify the most influential input parameters and to identify which input parameters have little or no effect on the conservatism [6]. In this technique, an emulator of the model is created by fitting a Gaussian Process (GP) to the response surface using data from multiple runs of the model as dictated by a Design of Experiments (DOE) so that the output of the model can be predicted for any point in the input space without having to run the simulation. Each input parameter is represented as a probability distribution and sensitivity analysis data is inferred at a reduced computational cost and with little loss of accuracy. Computational savings can be up to two orders of magnitude compared to using a Monte Carlo method [7, 8]. Accuracy of the emulator model is dependent on the model and the number of model runs, and can be quantified through cross-validation with the model runs.

This paper first describes the loads of interest when determining the serviceability of the Main Landing Gear (MLG) structure. The FPSS model is then explained. The theoretical background of the Bayesian sensitivity analysis is then presented, including a discussion on Gaussian Processes which are used to develop the emulator, and the main effects and sensitivity indices inferred from the resulting distribution-over-functions. Finally, the results of the sensitivity analysis for symmetric and asymmetric landings using the FPSS model are shown.

II. Landing Gear Loads

Figure 1 shows a typical aircraft and telescopic port MLG structure, with the sign conventions used in this paper. Figure 2 illustrates the landing dynamics of the port MLG in a two-point, symmetric landing. The starboard MLG landing dynamics are identical to the port MLG in a symmetric landing. On approach, the landing gear wheels are not spinning. However, on contact with the runway, the landing gear wheels spin-up to the ground speed of the aircraft under the influence of the ground reaction and the tire-runway friction. The resulting drag force deforms the landing gear aft and stores energy in the structure. When the tire velocity reaches the aircraft forward speed, the frictional force between the tire and the ground reduces and the release of the strain energy stored in the rearward deformation produces a spring-back. The landing gear oscillates until the structural damping reduces the stored energy to zero [9]. Also during this time, there is an increasing vertical ground-to-tire load, which is a function of the gas spring, oil damping (related to the square of the vertical descent velocity) and bearing friction. The shock absorber continues to close until all the vertical energy has been absorbed and then it partially recoils [10]. The shock absorber travel (SAT), in conjunction with aircraft attitude, landing gear rake angle and landing loads, creates a bending moment on the landing gear structure which is computed at the lower bearing. There are no side ground-to-tire loads developed in a symmetric landing. However, CS 25.485 does require side loads to be considered in design to account for landings with some degree of asymmetry [1].

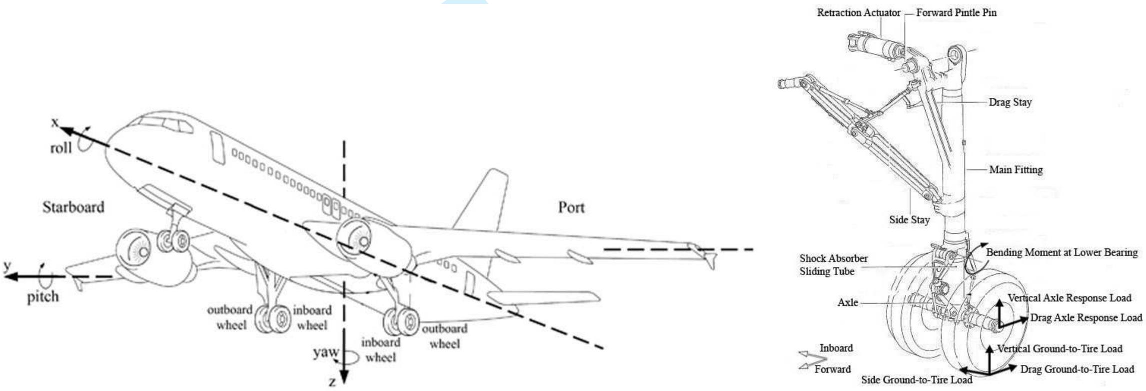

Fig. 1 Typical Aircraft and Port Main Landing Gear Structure with Sign Convention

In order to calculate the internal landing gear loads and assess the serviceability of the landing gear structure after a hard landing, the axle response loads are required. The ground-to-tire loads, discussed previously, act as the forcing function and with the mass and flexibility characteristics of the landing gear, produce the dynamic response loads at the landing gear axle. The difference between the ground-to-tire loads and the axle dynamic response loads is due to the inertial forces of the landing gear mass between the ground and the landing gear axle during the impact [11].

An asymmetric landing with aircraft lateral velocity, roll and yaw affects the landing dynamics significantly on the port and starboard MLG compared to a symmetric landing. Figure 3 illustrates

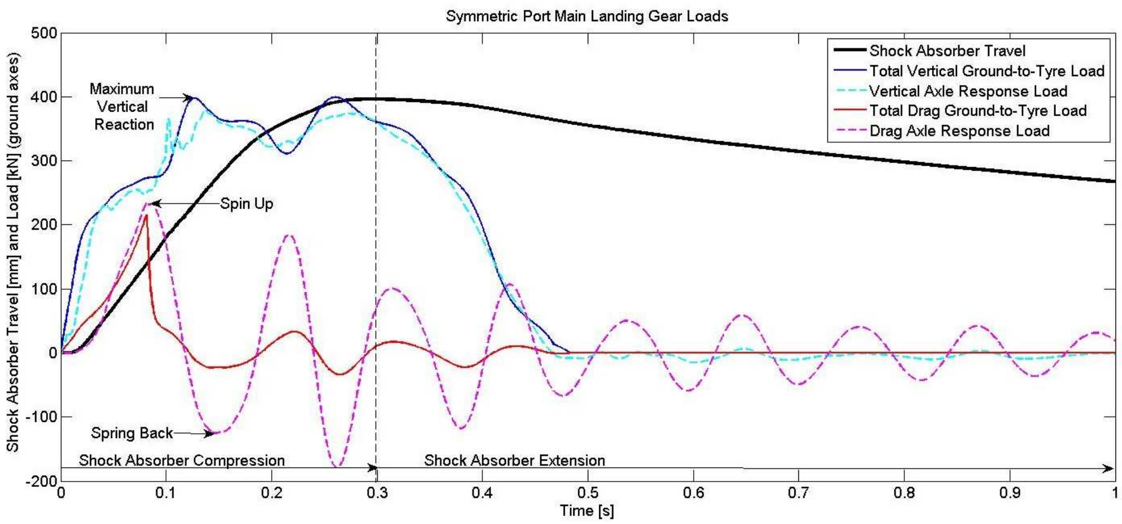

Fig. 2 Example of Symmetric Port Main Landing Gear Landing Dynamics

the MLG port and starboard loads from an asymmetric landing with only a positive initial aircraft lateral velocity and no roll or yaw angle. The initial aircraft lateral velocity acts in the starboard direction and on touchdown, the aircraft decelerates with a lateral acceleration that acts in the port direction, as shown by the reaction of the side ground-to-tire load acting on each MLG. Although the MLG wheels touchdown at the same time, the starboard MLG has a higher vertical ground-to-tire load than the port MLG. For a greater initial lateral velocity on landing, the aircraft lateral acceleration on impact with the ground increases. The magnitude of the vertical ground-to-tire load also increases on the starboard MLG, and decreases on the port MLG. However, the drag axle response load and bending moment do not significantly change as the lateral velocity defined in the initial conditions increases.

In a landing configuration with an initial negative aircraft roll angle, as illustrated in Figure 4, the aircraft is rolled with the port wing down so that the aircraft first lands on the port MLG and then on the starboard MLG. Therefore, the port MLG outer wheel touches down first, and carries more vertical load, followed by the port MLG inner wheel, which carries less of the vertical load. On the starboard MLG, the inner wheel touches down first, followed by the outer wheel.

For a greater initial roll angle on landing, the port MLG vertical load increases, while the starboard MLG load decreases. The fact that the MLG wheels touchdown at different times in landings with aircraft roll gives the distinctive total drag ground-to-tire curves with two peaks. As

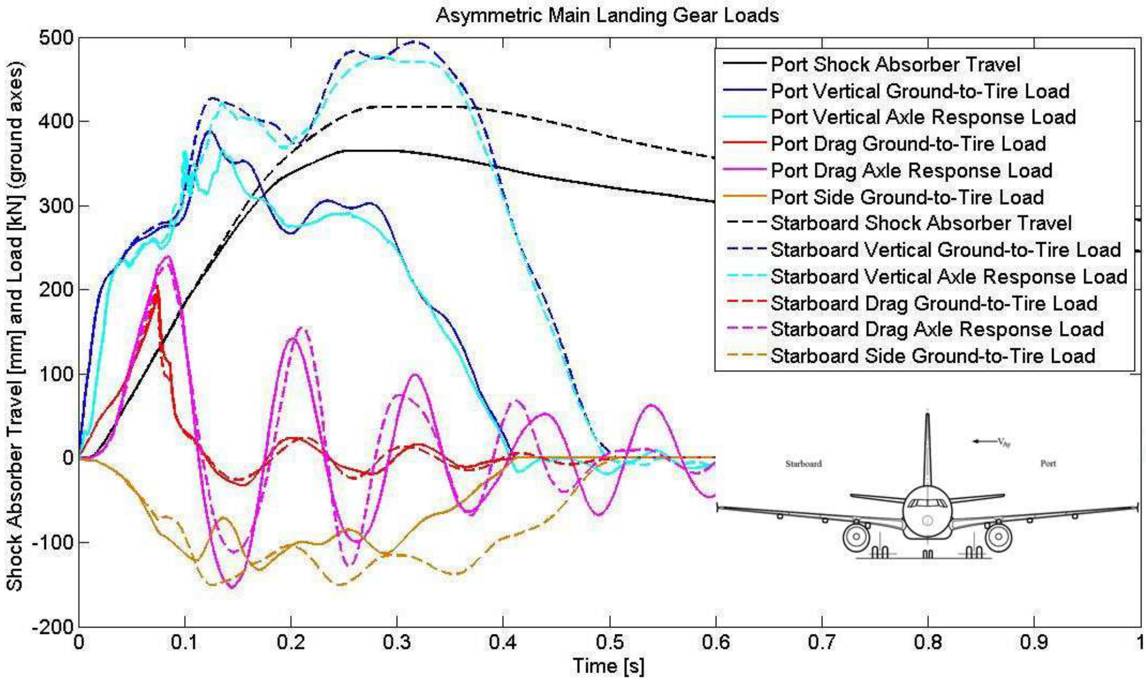

Fig. 3 Example of Asymmetric Main Landing Gear Loads Due to Aircraft Lateral Velocity

the initial aircraft roll angle increases, the total drag ground-to-tire load and the drag axle response load decreases. This is because the greater the roll angle, the greater the time between the wheels touching down and the build up of energy in the spin-up and spring-back is reduced.

Figure 5 illustrates the MLG port and starboard loads from an asymmetric landing with an initial aircraft positive yaw angle, yawed clockwise from the aircraft centreline. In this landing configuration, the aircraft decelerates with a lateral acceleration that acts in the starboard direction, as shown by the reaction of the side ground-to-tire load acting on each MLG. The port and starboard MLG wheels touchdown at the same time, however the port MLG has a higher vertical ground-to-tire load than the starboard MLG. For a greater initial yaw angle on landing, the port MLG vertical load increases, however, the starboard MLG vertical load decreases. The port MLG spin-up and spring-back drag axle response loads also decrease with increasing yaw angle.

The points of interest for the MLG landing analysis are the drag axle response load and bending moment at the lower bearing at spin-up and spring-back, and the vertical axle response load at maximum vertical reaction since these are the most sever loading cases that the MLG experience

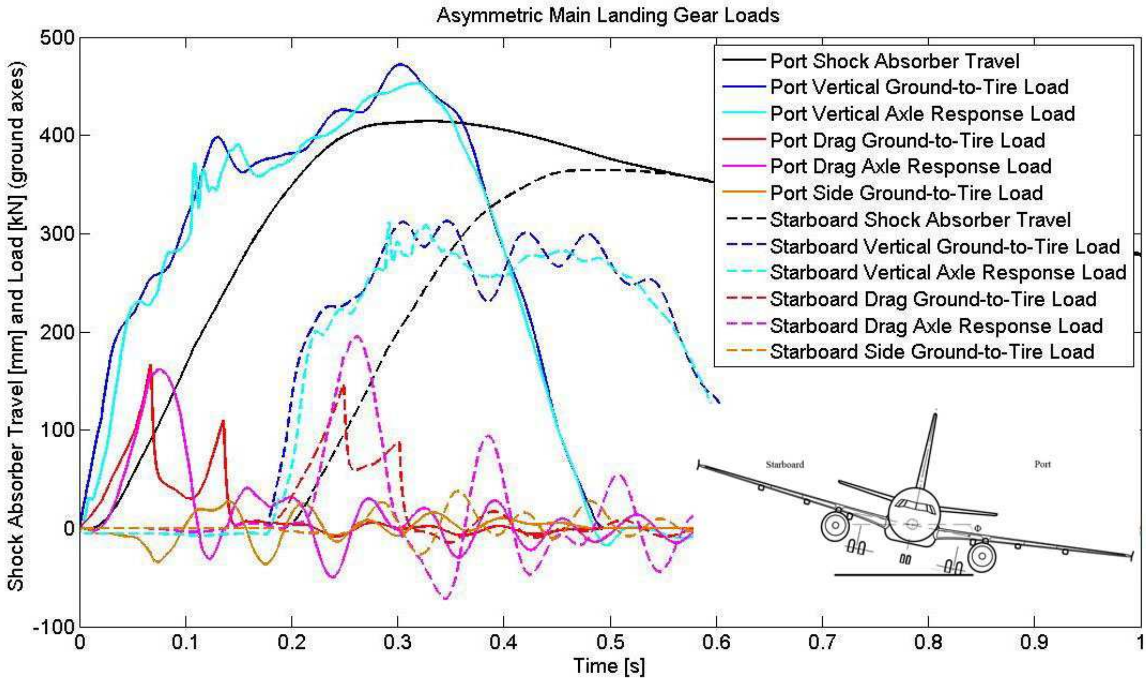

Fig. 4 Example of Asymmetric Main Landing Gear Loads Due to Aircraft Roll Angle

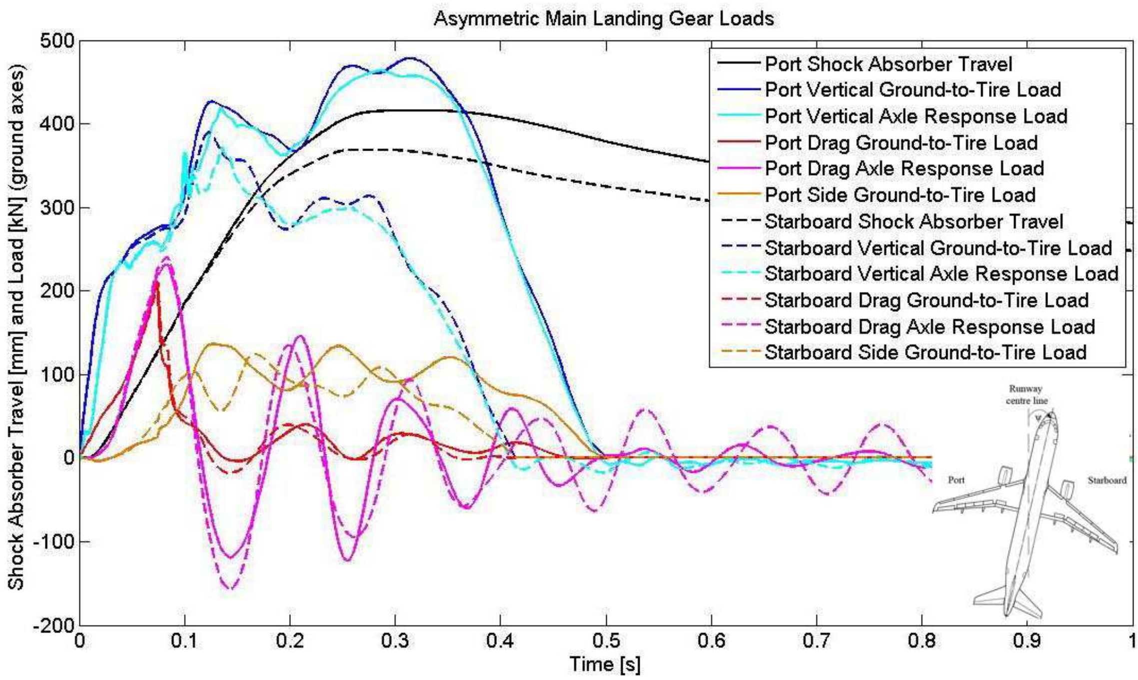

Fig. 5 Example of Asymmetric Main Landing Gear Loads Due to Aircraft Yaw Angle

on landing [12]. The side ground-to-tire load is of interest in asymmetric landings, however it will not be discussed in this paper.

III. Overview of the Flight Parameter Sensor Simulation Model

The FPSS model, shown in Figure 6, consists of: (1) an 'Actual' landing model to determine the 'actual' MLG loads during a hard landing, (2) an aircraft Sensor and Data Acquisition System Simulink model to represent the aircraft sensors and FDR systems to investigate the effect of signal processing on the flight parameters and (3) an automated Hard Landing Analysis Process model, representative of that used by airframe and landing gear manufacturers, to determine the 'simulated' MLG loads. Various hard landing cases were modelled using a representative aircraft and landing gear dynamic model. For each of the landing cases, it was possible to define flight parameters such as: aircraft mass ($mass$), aircraft centre of gravity location (CG), aircraft Euler pitch (θ), roll (ϕ) and yaw (ψ) angles, aircraft longitudinal velocity (V_{A_x}), vertical descent velocity (V_{A_z}), lateral velocity (V_{A_y}), MLG shock absorber servicing state ($Port\ SA$, $Starboard\ SA$), tire type ($tire$), tire pressure ($tire\ press$) and the longitudinal and lateral tire-runway friction coefficients (μ_{long}, μ_{lat}). These landing cases provide simulation of the 'actual' flight parameters, as well as the 'actual' landing gear loads at spin-up, spring-back and maximum vertical reaction.

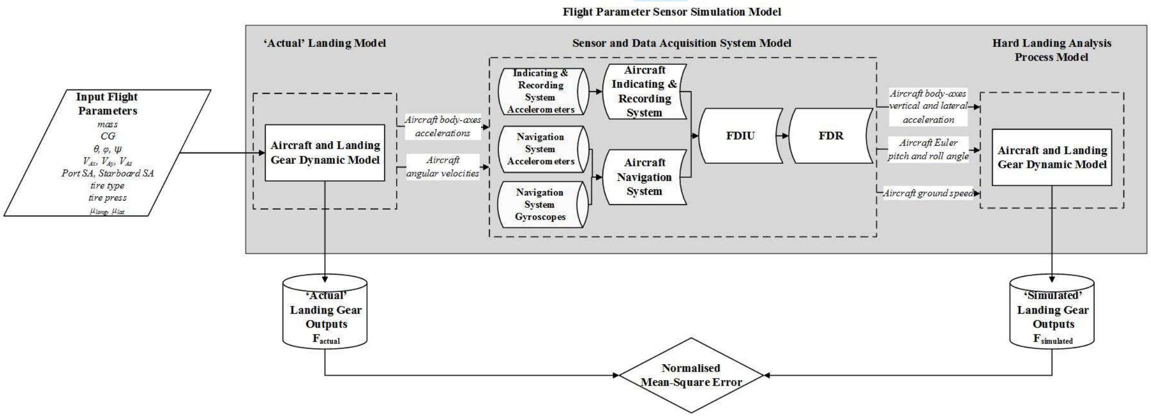

Fig. 6 Flight Parameter Sensor Simulation Model

The aircraft sensor and data acquisition model represents the aircraft sensors and FDR systems. Aircraft flight parameters such as vertical and lateral accelerations, Euler pitch and roll angle and aircraft longitudinal velocity are used in the typical hard landing analysis process. A typical aircraft Indicating & Recording system, Navigation system, Flight Data Interface Unit (FDIU) and Flight Data Recorder (FDR) was modelled in Simulink to investigate the effect of signal processing (sampling rate, filtering, analog to digital conversion, transfer/receive delays) on the aircraft flight parameters.

Finally, with the flight parameter data from the FDR, a hard landing analysis process, representative of that used by airframe and equipment manufacturers, was modelled and the conservative assumptions typically made were applied. These assumptions include: aircraft mass, inertia and centre of gravity location as close as possible to the occurrence case, assumed tire type, correctly serviced shock absorber (correct fluid volume and gas pressure) and assumed tire-runway friction coefficient. The peak aircraft vertical acceleration data from the FDR, as well as the other FDR parameters at the peak vertical acceleration, are used to model the landing gear loads. Based on the initial conditions provided by the FDR (Euler pitch and roll angles, aircraft longitudinal velocity), the aircraft vertical descent velocity was iterated until the aircraft vertical acceleration output from the hard landing analysis process model matched the peak vertical acceleration from the FDR. In the Hard Landing Analysis Process model, the MLG side ground-to-tire loads are calculated using a bookcase calculation method (footnote:Bookcase calculations, as given in CS 25, tend to be more artificial and usually require ground reactions to be balanced by inertia forces and moments. Rational calculations use a model that more accurately represents the real physics and dynamics of the system [9].): a ground manoeuver turn using the lateral acceleration ($LATG$) at the peak $VRTG$, where the side ground-to-tire load is a function of $LATG$ and the drag and vertical ground-to-tire loads are factored as a function of $LATG$.

In the FPSS model, the Aircraft and Landing Gear Dynamic model used in the 'Actual' Landing model and the Hard Landing Analysis Process model are the same. Therefore, the 'simulated' landing perfectly models the 'actual' landing and there is no error due to modelling. Any differences in the 'actual' and 'simulated' landing gear loads are due to the conservative assumptions in the hard landing analysis process and loss of data content from the FDR systems and processing algorithms.

From the landing gear loads calculated based on those conditions, it was possible to estimate the conservatism between the 'actual' landing gear output (F_{actual}) and the 'simulated' ($F_{simulated}$)

landing gear output using a normalised mean-square error (MSE) method [8]:

$$MSE = \frac{(F_{actual} - F_{simulated})^2}{\sigma^2_{F_{actual}}} \times 100 \quad (1)$$

where $\sigma^2_{F_{actual}}$ is the variance of F_{actual} from all of the model runs.

Table 1 provide a summary of the model inputs and outputs for symmetric and asymmetric landings. As discussed in Section II, the points of interest for the MLG landing analysis are the drag axle response load and bending moment at the lower bearing at spin-up and spring-back, and the vertical axle response load at maximum vertical reaction. Therefore the MSE is calculated for these outputs.

Landing	Input Flight Parameters	Output Quantity
Symmetric	θ, V_{A_x}, V_{A_z}, $Port\ SA$, $mass$, CG, $tire$, $tire\ press$, μ_{long}	Spin-up and Spring-back Drag Axle Response Load MSE, Spin-up and Spring-back Bending Moment MSE, Maximum Vertical Axle Response Load MSE
Asymmetric	θ, ϕ, ψ, V_{A_x}, V_{A_z}, V_{A_y}, $Port\ SA$, $Starboard\ SA$, $mass$, CG, $tire$, $tire\ press$, μ_{long}, μ_{lat}	Spin-up and Spring-back Drag Axle Response Load MSE, Spin-up and Spring-back Bending Moment MSE, Maximum Vertical Axle Response Load MSE

Table 1 Summary of Flight Parameter Sensor Simulation Model Inputs and Outputs

IV. Bayesian Sensitivity Analysis Theory

This section presents the theoretical background of the Bayesian sensitivity analysis, including a discussion on GPs which are used to develop the emulator, and the main effects and sensitivity indices inferred from the resulting distribution-over-functions.

A. Gaussian Processes

Any computer model, such as the FPSS model, can be considered a function of its inputs: $f(\mathbf{x})$. Although this function is deterministic and governed by known mathematical functions, it is often complex and may be encoded by a large numerical model which has no closed-form expression for its outputs as a function of its inputs. Therefore, $f(\mathbf{x})$ could be considered an unknown function, since the output is unknown for a given set of inputs until the model has actually been run. If however, the function (model) is sampled at a number of carefully chosen input points, it is possible to fit a response surface (footnote: A response surface is the hypersurface of the model output as a result of varying the inputs [13].) which can predict the output of the model for any point in the input space without having to run the model. For models that are computationally expensive (i.e. they require several minutes, hours or days to run), creating a fast-running emulator (a model of a model) is a useful approach for sensitivity analysis which generally requires multiple runs of the model under investigation [7]. To be successful the emulator must be general and as little as possible must be assumed about the emulator function. The emulator should also be able to accurately imitate the model using as few training points as possible [13].

A particular probabilistic approach for developing an emulator is the use of Gaussian Process (GP) regression [14–16]. GPs assume that observations $f(\mathbf{x}_1)$, $f(\mathbf{x}_2)$,. . . ,$f(\mathbf{x}_n)$, as well as unobserved values of f, are distributed joint-normally, i.e. they can be represented by a multivariate Gaussian distribution. This means that predictions at unobserved values of $\mathbf{x}$ are also returned as a Gaussian distribution. The mean and variance at any point are specified by a mean function and a covariance function, which are functions of $\mathbf{x}$, as well as a number of hyperparameters. Another way of looking at a GP is a distribution-over-functions, where the random variable of the distribution is a function rather than a single number or a fixed-length vector [13].

The covariance function typically has the property that the predictive variance increases for values of $\mathbf{x}$ that are further away from training data. This means that the predictive variance of a GP is a function of the distance to known points. It is useful to contrast this to linear regression, which may also give normally-distributed estimates at unobserved points. The difference is however that in linear regression, the data points are assumed to be noisy, whereas a GP exactly interpolates though the training data. In linear regression therefore, probabilistic predictions usually reflect noise in the training data, or parameter uncertainty (especially within the Bayesian framework).

GPs adhere to the Bayesian paradigm, such that a number of prior assumptions are made about the function being modelled, and then training data (samples from the model) are used to update and evaluate a posterior distribution-over-functions. It is assumed that the model is a smooth function so that if the value of $f(\mathbf{x})$ is known, the value at $f(\mathbf{x}')$ for $\mathbf{x}$ close to $\mathbf{x}'$ will be highly correlated [7]. This assumption allows information to be gained on the response surface at reduced computational cost.

For any number of d model input parameters, each with n training data points, the prior beliefs about the corresponding outputs can be represented by a multivariate normal distribution, the mean of which is a least-squares regression fit through the training data [7]:

$$m(\mathbf{x}) = E\{f(\mathbf{x})|\mathbf{w}\} = \mathbf{h}(\mathbf{x})^T\mathbf{w} \tag{2}$$

where $\mathbf{h}(\mathbf{x})^T$ is a specified vector of q regression functions of $\mathbf{x}$, and $\mathbf{w}$ is the corresponding q-length vector of coefficients. Here, $\mathbf{h}(\mathbf{x})^T$ is chosen to be $(1, \mathbf{x}^T)$, which represents linear regression. This is a reasonable assumption since many engineering models display roughly linear behavior with respect to at least some of the model inputs [13]. Here the covariance between output points is defined by a squared-exponential function of the form [7]:

$$cov\{f(\mathbf{x}), f(\mathbf{x}')|\sigma^2\} = \sigma^2 c(\mathbf{x}, \mathbf{x}') = \sigma^2 exp\{-(\mathbf{x}-\mathbf{x}')^T B(\mathbf{x}-\mathbf{x}')\} \tag{3}$$

where σ^2 is a scaling factor of the GP covariance function and B is a diagonal matrix of length-scales, which represent the roughness of the output (in terms of correlation length-scales as opposed to differentiability) with respect to the individual input parameters. The hyperparameters, $\mathbf{w}$, σ^2, B, are the controlling parameters that define the behavior of the emulator, which allows the emulator to be general enough for a wide range of engineering problems [13]. The squared-exponential covariance function is by no means the only covariance function - many others are detailed in Rasmussen and Williams [17]. The squared-exponential function imposes an assumption of derivatives of all orders, which may be a strong assumption for a physical model. An alternative could be the more flexible Matérn class of functions, however within the context of this work, the squared-exponential functions have the advantage of being sufficiently tractable to provide analytic expressions for sensitivity indices. Furthermore, the added flexibility of the Matérn functions also comes at the cost of having more parameters to estimate. Testing of more sophisticated covariance functions is a valid avenue of enquiry but is left as future work.

The prior distribution is then defined as [13]:

$$f(\mathbf{x}) \sim GP(m(\mathbf{x}), \sigma^2 c(\mathbf{x}, \mathbf{x}')) \tag{4}$$

where $\sim$ means distributed as.

The posterior distribution is then found by conditioning the prior distribution on the training data on $\mathbf{y}$ (the output vector corresponding to the input set), and integrating out the hyperparameters σ^2 and $\mathbf{w}$. This results in a Student's t-process, conditional on B and the training data [13]:

$$[f(\mathbf{x})|B, \mathbf{y}] \sim t_{n-q}\{m^*(\mathbf{x}), \hat{\sigma}^2 c^*(\mathbf{x}, \mathbf{x}')\} \tag{5}$$

where $m^*(\mathbf{x})$ and $c^*(\mathbf{x}, \mathbf{x}')$ are the posterior mean and covariance function respectively, which are only dependent on B and $\mathbf{y}$ - expressions for these can be found in [7]. Note that as a result of the integration, the posterior distribution is no longer dependent (conditional) on σ^2 and $\mathbf{w}$, and now incorporates uncertainty about their values. This is where the benefit of the squared-exponential covariance function is apparent - the analytical integration avoids approximations via numerical methods such as Markov Chain Monte Carlo, which introduce their own uncertainty. The roughness parameters in B are estimated using maximum likelihood estimation, since they appear to be too difficult to analytically marginalise. In this respect, the GP is not fully Bayesian, and uncertainty in B is not accounted for in the posterior distribution. The quality of the emulator is dependent on the number and distribution of training data points in the input space, and the values of the hyperparameters.

B. Inference for Sensitivity Analysis

If the input vector, $\mathbf{x}$, is uncertain, $\mathbf{X}$, the “true input configuration" is considered a random variable with the distribution $p(\mathbf{x})$ [7]. The output $Y = f(\mathbf{X})$ is then also a random variable and the distribution of Y is known as the uncertainty distribution. With the emulator defined by the posterior distribution-over-functions described by Equation 5, several quantities relevant to the sensitivity analysis can be analytically derived without the necessity of additional model runs: the main effects and interactions, as well as the sensitivity measures including Main Effects Indices (MEI) and Total Effects Indices (TEI). In order to estimate the sensitivity measures, an assumption is made that the input parameters are independent.

1. Main Effects

The function $f(\mathbf{x})$ can be decomposed into main effects and interactions [18]:

$$y = f(\mathbf{x}) = E(Y) + \sum_{i=1}^{d} z_i(\mathbf{x}_i) + \sum_{i<j}^{d} z_{i,j}(\mathbf{x}_{i,j}) + \sum_{i<j<k}^{d} z_{i,j,k}(\mathbf{x}_{i,j,k}) + \ldots + z_{1,2,\ldots,d}(\mathbf{x}) \tag{6}$$

$$z_i(\mathbf{x}_i) = E(Y|\mathbf{x}_i) - E(Y) \tag{7}$$

$$z_{i,j}(\mathbf{x}_{i,j}) = E(Y|\mathbf{x}_{i,j}) - z_i(\mathbf{x}_i) - z_j(\mathbf{x}_j) - E(Y) \tag{8}$$

Here $z_i(\mathbf{x}_i)$ represents the main effect of $\mathbf{x}_i$, which is the effect (on the output) of varying that parameter over its input range, averaged over all the other inputs. The main effects of the input parameters are are normalised onto the unit interval and plotted. Main effects plots are graphical representations that show the expected value of the output obtained by averaging all other inputs, except the one considered, and provide information on which model inputs the output is sensitive to and the nature of the input-output relationships [19]. The main effects plots do not consider the interactions with other flight parameters therefore the plots do not show the value of the MSE at a particular value of the input parameter. In Equation 8, $z_{i,j}(\mathbf{x}_{i,j})$ is the first order interaction between x_i and x_j, which describes the effect of varying two or more parameters simultaneously, additional to the main effects of both parameters. The terms $z_{i,j,k}(\mathbf{x}_{i,j,k}),\ldots,\ z_{1,2,\ldots,d}(\mathbf{x})$ represent higher-order interactions. $E(Y)$ is the expected value of the output y considering all possible combinations of inputs.

The posterior mean values for main effects and interactions can be inferred by substituting the posterior mean from Equation 5 into the conditional expectation:

$$E(Y|\mathbf{x}_i) = \int_{\chi_{-i}} f(\mathbf{x}) p(\mathbf{x}_{-i}|\mathbf{x}_i) d\mathbf{x}_{-i} \quad (9)$$

where χ_{-i} is the sample space of $\mathbf{x}_{-i}$, $\mathbf{x}_{-i}$ is the subvector of $\mathbf{x}$ containing all elements except $\mathbf{x}_i$ and $p(\mathbf{x})$ represents the multivariate probability distribution of the input parameters. Although this results in a series of matrix integrals, a Gaussian or uniform $p(\mathbf{x})$ distribution, combined with a sufficiently tractable covariance function (such as the squared exponential function used in this work), allows these to be solved analytically. Expressions for interactions can also be derived with their respective definitions.

2. Variance and Sensitivity Indices

In Reference [7], variance-based methods of probabilistic sensitivity analysis are described in order to quantify the proportion of output variance for which individual input parameters are responsible. In particular, sensitivity can be measured by conditional variance:

$$V_i = var\{E(Y|X_i)\} \quad (10)$$

For interpretation, this variance measure can be standardized by dividing the total output variance:

$$S_i = \frac{V_i}{var(Y)} = \frac{var\{E(Y|X_i)\}}{var(Y)} \quad (11)$$

where S_i is the Main Effect Index (MEI) of x_i, a widely-used global sensitivity measure proposed by Sobol' [18]. MEIs represent the fractional contribution of individual inputs to the uncertainty (variance) of the model output. A high MEI means the variance of the output will be reduced considerably if we learn the "true" value of the input flight parameter. This idea can be extended to measure conditional variance of interactions of inputs, for example first order interactions $V_{i,j} = var\{z_{i,j}(\mathbf{x}_{i,j})\}$, which is the effect of varying two input flight parameters simultaneously, additional to the main effects of both parameters, and so on for higher order interactions. Therefore, summing the main effects will not in general total one because of the contributions from the interactions. However, the total does provide an indication of the degree of the interactions [19].

An additional sensitivity measure gives the variance caused by an input x_i and any interaction of any order including x_i and describes the output variance that would remain if one were to learn the true values of all inputs except x_i:

$$V_{Ti} = var(Y) - var\{E(Y|\mathbf{X}_{-i})\} \tag{12}$$

After standardization this gives:

$$S_{Ti} = \frac{V_{Ti}}{var(Y)} = \frac{var(Y) - var\{E(Y|\mathbf{X}_{-i})\}}{var(Y)} \tag{13}$$

where S_{Ti} is known as the Total Effects Index (TEI) [20]. The TEI includes the interactions with every input flight parameter associated with it and therefore, considering all d TEIs of all variables, may be counted twice for an interaction between two variables, three times for an interaction between three variables, etc. Therefore, the TEIs may sum to more than one.

In [7], it is shown how the GP metamodel can be analytically integrated to give estimates of both V_i and V_{Ti}, without the need for a Monte Carlo sampling procedure from the metamodel (as is used in most metamodel-based sensitivity analyses). The details of these integrals, which are quite complex, are left to [7]. All the quantities of interest presented here are calculated using the software package Gaussian Emulation Machine for Sensitivity Analysis (GEM-SA) [21].

Note that a number of other approaches to sensitivity analysis exist in the literature that use GPs and other emulators to perform uncertainty and sensitivity analysis. For example, the method presented in [22] considers multifidelity computer codes and is implemented in the R package "sensitivity". In addition, the "tgp" package [23] offers a greater flexibility by generalising GPs using regression trees, allowing emulation of nonstationary models and bifurcating responses [24]. However for the purposes of this work, the more "standard" GP was considered sufficient, given that there is no particular reason to suspect bifurcations in the mode here. This assumption appears to be justified by the cross-validation results in Section V A.

V. Sensitivity Analysis of Flight Parameter Sensor Simulation Model

The Bayesian sensitivity analysis technique described in Section IV has been used to examine the sensitivity of models in a variety of disciplines including: Bouc-Wen model of hysteresis [25], soil-vegetation-atmospheric transfer [19], nuclear radiation releases [14], vehicle crashes, spot welding [26] and the aortic valve [13]. The Bayesian sensitivity analysis technique is considered to be well-tested, robust and useful [19].

Using this Bayesian sensitivity analysis technique, a number of flight parameters are varied in the FPSS model, described in Section III, to gain an understanding of the sensitivity of the input flight parameters to the difference in the 'actual' and 'simulated' loads, calculated as Mean-Square Error (MSE), due to the signal processing in the Sensor and Data Acquisition model and the assumptions and inaccuracies in the Hard Landing Analysis Process model. This is a novel application of the Bayesian sensitivity analysis technique to an aircraft landing gear model and it is the first time the MSE has been used to quantify the conservatism in a model.

Figure 7 provides a summary of the methodology followed in conducting the sensitivity analysis on the FPSS model using GEM-SA in this paper. The Bayesian sensitivity analysis technique in GEM-SA is comprised of two stages: the first involves creating an emulator of the FPSS model by fitting a GP to the response surface using data from multiple runs of the model as dictated by a Design Of Experiments (DOE) so that the output of the FPSS model can be predicted for any point in the input space without having to run the simulation. The second stage involves representing each input flight parameter as a probability distribution and using the emulator built in the first stage to infer sensitivity analysis data.

For symmetric, two-point landings, the nine input flight parameters to the 'Actual' Landing model include: θ, V_{A_x}, V_{A_z}, μ_{long}, *Port SA* (Footnote: For symmetric landings, the starboard MLG mirrors the port MLG therefore only the port MLG servicing state is specified.), *tire*, *tire press*, *mass* and *CG*. For asymmetric, two-point landings, the 12 input parameters to the 'Actual' Landing model include: ϕ, θ and ψ, V_{A_x}, V_{A_y}, (V_{A_z}), μ_{long}, μ_{lat}, *Port SA*, *Starboard SA*, *mass* and *CG*. The input parameters *tire* and *tire press*, that were considered in the symmetric landings, are not considered for the asymmetric landings because lateral tire data was only available for one tire at

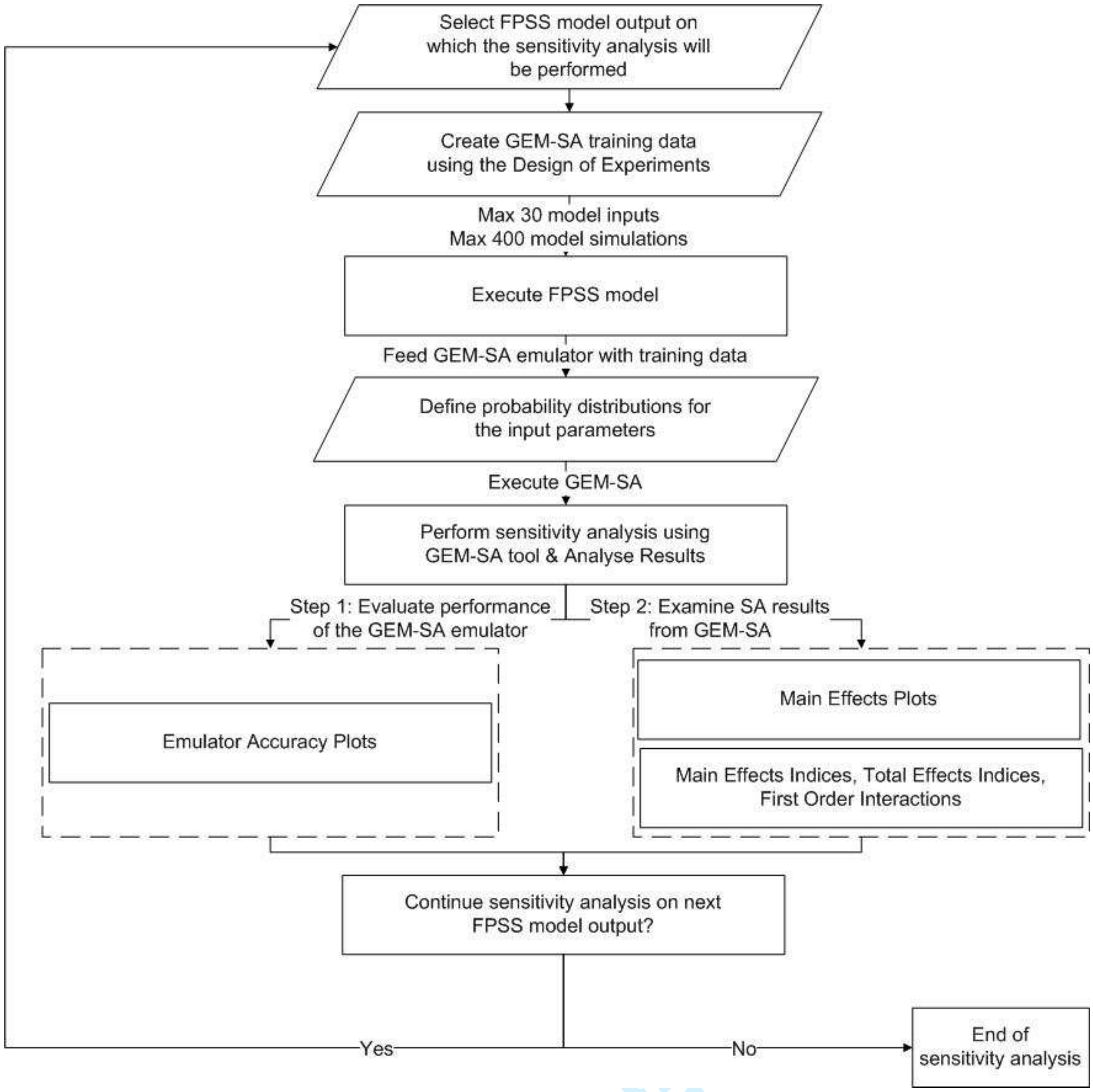

Fig. 7 Methodology Followed in Conducting the Sensitivity Analysis on the FPSS model using GEM-SA, after [19]

one tire pressure and therefore it was not possible to consider the other tire types or tire pressures.

In order to estimate the sensitivity measures described in Section IV, the probability distributions for the input parameters are defined. The assumption was made that the inputs are independent, although in reality flight parameters such as pitch and ground speed are not independent and flight parameters such as roll and yaw may be coupled. But given the limited range considered at landing, they are relatively independent. The parameters can be specified as either Gaussian or uniformly distributed based on how informative the available input parameter data are. In this study, the distributions have been defined as uniform distributions and the ranges of the flight parameters, normalized between zero and one, are based on typical aircraft operating limitations.

To develop the emulator, 400 combinations of input parameters were generated using a maximin Latin Hypercube DOE in GEM-SA. The FPSS model was then run to provide the corresponding 'actual' and 'simulated' landing gear outputs calculated at spin-up, spring-back and maximum vertical reaction. The outputs of interest are: spin-up and spring-back drag axle response load MSE, spin-up and spring-back bending moment MSE and maximum vertical reaction vertical axle response load MSE. The sensitivity analysis was carried out in GEM-SA.

For symmetric landings, the port and starboard MLG give the same results, therefore only the port MLG results are presented, however, for asymmetric landings, the port and starboard MLG provide different results, therefore both MLG were considered in the sensitivity analysis.

A. Emulator Accuracy

For each sensitivity study, the emulator is built on the first 80% of the training data and the accuracy of the emulator is evaluated using the remaining 20% of the training data. Since the emulator calculates a mean function, which passes through the outputs and also quantifies the remaining uncertainty due to the emulator being an approximation of the true model, the emulator accuracy is evaluated graphically using the emulator predictions and their 95% confidence bands, as well as the model output data (data not used in training). Figure 8 and Figure 9 shows an example of the emulator accuracy for the asymmetric landing port and starboard spin-up drag axle response load MSE. The model test data tended to be within the 95% confidence bands of the predictions and errors could be attributed to predicting high values of MSE since there are fewer training points for the emulator in these regions.

GEM-SA also provides other statistical measures of the emulator accuracy, including "roughness" values for the input flight parameters, a σ^2 value and cross-validation root mean square (RMS) error. The roughness values, related to the hyperparameter B, estimate the smoothness of the model inputs and describes how quickly the output responds to changes in each input [19]. Roughness values greater than one indicate non-linear relationships between the inputs and outputs,

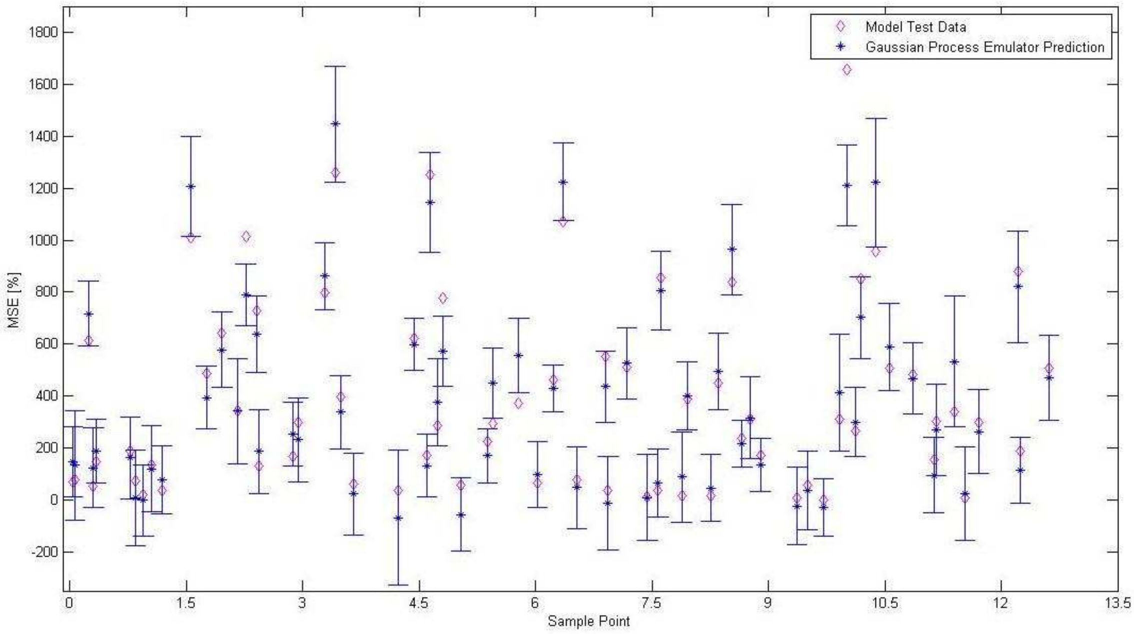

Fig. 8 Asymmetric Port MLG Spin Up Drag Axle Response Load Emulator Accuracy

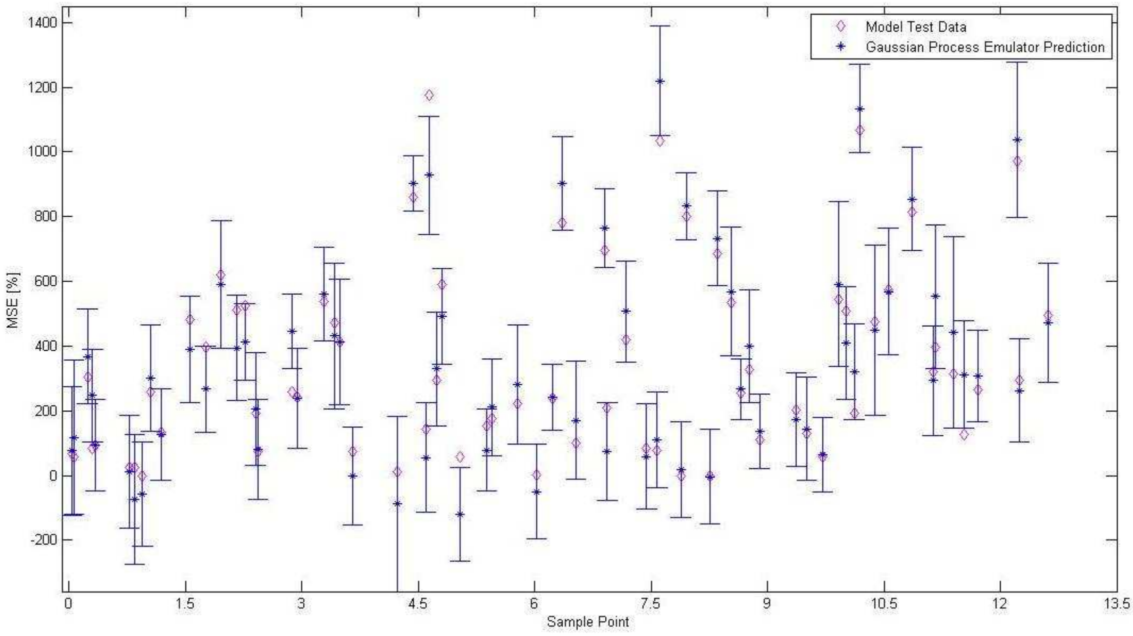

Fig. 9 Asymmetric Starboard MLG Spin Up Drag Axle Response Load Emulator Accuracy

while roughness values approaching 100 indicate discontinuities and suggest that the emulator is not working. The σ^2 value provides the variance of the emulator after standardizing the output and provides a measure of the non-linearity in the emulator [19]. Finally, the cross-validation RMS error is the square root of the mean square error of the emulator predictions at the training points [19].

The statistical measures of the emulator accuracy for the asymmetric landing port and starboard MSE sensitivity analyses are presented in Table 2 and Table 3. Since the port and starboard MLG emulators are trained with different data, the roughness values, σ^2 values and RMS errors are different.

Roughness values for all of the input parameters, for both the port and starboard MLG, are below 10, except for the input parameter μ_{long}, which had a roughness value of 30.42 for the starboard spring-back drag axle response load MSE output. Therefore, the emulators generally had a smooth response to variations in its input and are good approximations to the FPSS model. While the roughness value for μ_{long} is high, it does not suggest extremely non-linear or discontinuous patterns. However it does suggest that μ_{long} is one of the sensitive inputs. Roughness values are also greater than one in some cases for ϕ, $V^e_{A_z}$, $V^e_{A_y}$ and $mass$, which indicates that these are the most sensitive input parameters. Roughness values are consistently less than one for input parameters such as *Port SA* and *Starboard SA*, indicating linear relationships between the inputs and outputs. The σ^2 values for each of the SA are low and range from 0.77-2.70 for the port MLG and 0.76-2.83 for the starboard MLG, which means that the parameters only moderately deviate from linearity [19]. The RMS error is not normalized but is expressed in terms of the output. Therefore, when the RMS error is taken in context to the data in the emulator accuracy plots, it is acceptable. These results suggests that the emulator is a good representation of the FPSS model.

B. Main Effects Plots

The main effects plots for the analysis show MSE versus the normalised flight parameters. The lines represent mean main effects values, averaged over variations in the other parameters and can be thought of as the expected value of the output with respect to one parameter if the true values of the other parameters are known. These plots show which of the flight parameters the MSE is significantly sensitive to and the nature of the input/output relationships.

The main effects plots for the port and starboard MLG are related such that parameters in the aircraft x and z axes, such as θ, V_{A_x}, V_{A_z}, μ_{long}, *Port SA*, *Starboard SA*, *mass* and *CG* show the same trend for both landing gears. However, for parameters such as ϕ, ψ and V_{A_y} the main

Flight Parameter	Roughness				
	Drag Axle Response Load		Bending Moment		Vertical Axle Response Load
	Spin-Up	Spring-Back	Spin-Up	Spring-Back	Maximum Vertical Reaction
ϕ	1.25	2.37	1.31	5.37	1.14
θ	0.51	1.94	0.30	1.79	0.96
ψ	0.33	0.53	1.87	2.39	0.05
V_{A_x}	0.47	1.77	0.11	0.00	0.04
V_{A_y}	1.18	0.80	3.29	5.01	0.58
V_{A_z}	1.47	3.38	0.79	0.69	5.29
μ_{long}	2.52	9.95	1.08	0.63	0.29
μ_{lat}	0.96	0.73	0.81	0.86	0.09
Port SA	0.21	0.00	0.01	0.15	0.01
Starboard SA	0.03	0.19	0.01	0.25	0.02
mass	0.13	0.30	1.10	1.01	3.62
CG	0.14	0.25	0.13	0.16	1.51
Fitted model parameters					
σ^2	0.91	0.77	1.76	1.26	2.70
Cross Validation Results					
Cross Validation RMS Error [%]	106.86	138.26	248.22	239.51	17.37
Cross Validation RMS Standardized Error	1.33	1.49	1.27	1.33	1.13

Table 2 Asymmetric Port Main Landing Gear MSE Emulator Accuracy

effects plots are mirrored. Not surprisingly, the input parameters that were also investigated in the symmetric landing sensitivity analysis (θ, V_{A_x}, V_{A_z}, μ_{long}, *Port SA*, *mass* and *CG*) show the same trends in the asymmetric landing sensitivity analysis main effects plots. This provides additional verification that the FPSS model is performing correctly for asymmetric landings.

The symmetric landing main effects plots for drag axle response load MSE and bending moment MSE at spin-up and spring-back show the same trends therefore only the spin-up drag axle response load MSE main effects plots are shown in Figure 10. The symmetric landing maximum vertical reaction vertical axle response load main effects plots are shown in Figure 11. The main effects plot for *tire* was not illustrated because a discrete uniform distribution was assigned to each tire. In GEM-SA, this was described by a continuous distribution and the main effects plots are not meaningful.

The asymmetric landing main effects plots for port and starboard MLG drag axle response load MSE, bending moment MSE at spin-up and spring-back, and maximum vertical reaction vertical

Flight Parameter	Roughness				
	Drag Axle Response Load		Bending Moment		Vertical Axle Response Load
	Spin-Up	Spring-Back	Spin-Up	Spring-Back	Maximum Vertical Reaction
ϕ	0.26	1.80	0.68	5.62	0.35
θ	0.56	0.89	0.33	0.50	1.19
ψ	0.58	0.14	1.00	1.54	0.26
V_{A_x}	0.80	2.89	0.61	0.08	0.26
V_{A_y}	1.00	0.33	2.86	2.53	0.27
V_{A_z}	1.58	6.03	1.31	0.20	3.28
μ_{long}	3.26	30.42	1.53	0.95	0.11
μ_{lat}	1.32	0.18	1.08	0.38	0.13
Port SA	0.00	0.00	0.00	0.03	0.28
Starboard SA	0.08	0.07	0.18	0.04	0.14
mass	0.27	0.23	0.42	1.53	5.27
CG	0.23	0.22	0.08	0.08	0.59
Fitted model parameters					
σ^2	0.90	0.76	1.62	2.83	2.78
Cross Validation Results					
Cross Validation RMS Error [%]	85.08	129.75	184.98	205.28	16.21
Cross Validation RMS Standardized Error	1.07	1.45	1.29	1.29	1.22

Table 3 Asymmetric Starboard Main Landing Gear MSE Emulator Accuracy

axle response load MSE show the same trends for the input parameters ϕ, ψ and V_{A_y} and μ_{long}. The spin-up drag axle response load MSE main effects plots for the asymmetric input flight parameters are shown in Figure 12.

1. *Aircraft Pitch Angle*

The symmetric and asymmetric main effects plots show that the spin-up and spring-back drag axle response load MSE and bending moment MSE increases as the pitch angle increases. Due to filtering and sampling, the Sensor and Data Acquisition model tends to contribute an error of the magnitude of less than one degree, therefore it is not expected that θ would have a large contribution to the MSE. Part of the relationship between θ and MSE can be attributed to the constraint in the model that limits the pitch angle to greater than 0 degrees to ensure a two-point landing. If this constraint is removed, the relationship between θ and MSE tends to be more constant. The main effects plot for the vertical axle response load MSE also shows a constant relationship with θ. Section V C will show that the contribution to the MSE from θ alone is low, except in the case of

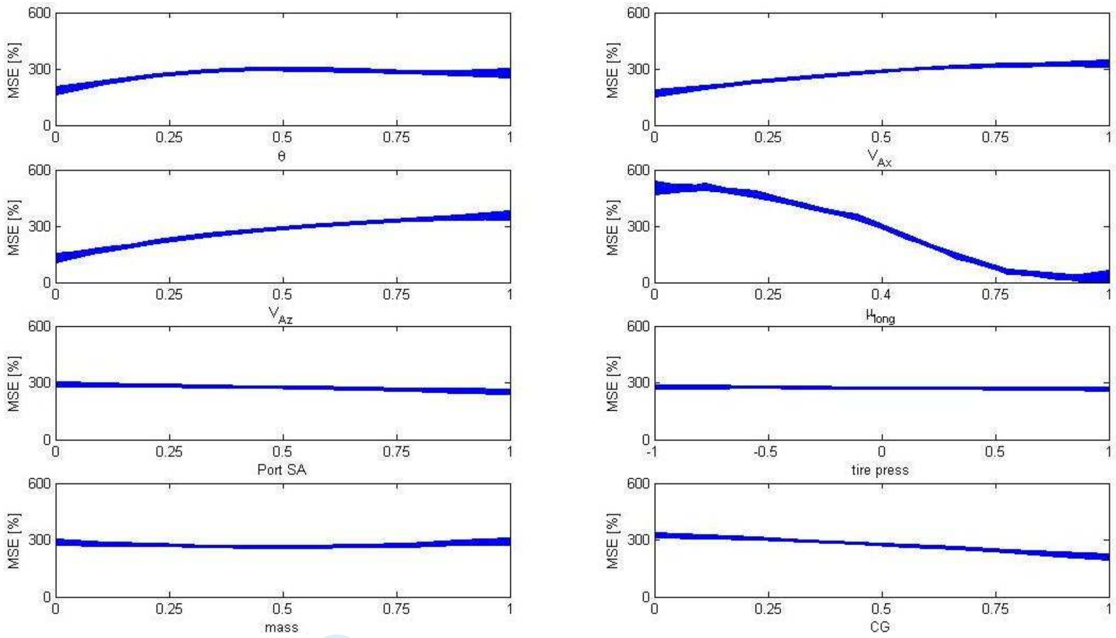

Fig. 10 Symmetric Port MLG Spin Up Drag Axle Response Load Main Effects Plots

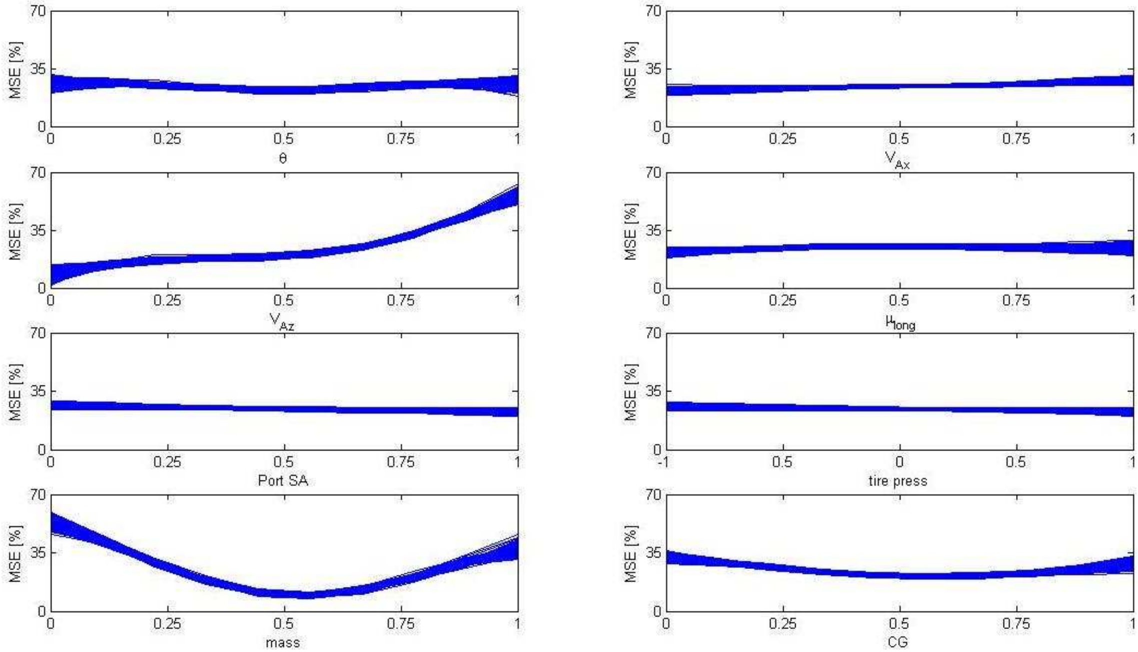

Fig. 11 Symmetric Port MLG Maximum Vertical Reaction Vertical Axle Response Load Main Effects Plots

spring-back bending moment MSE. The flight parameter θ tends to only be significant in the other cases when its interactions with other flight parameters are considered.

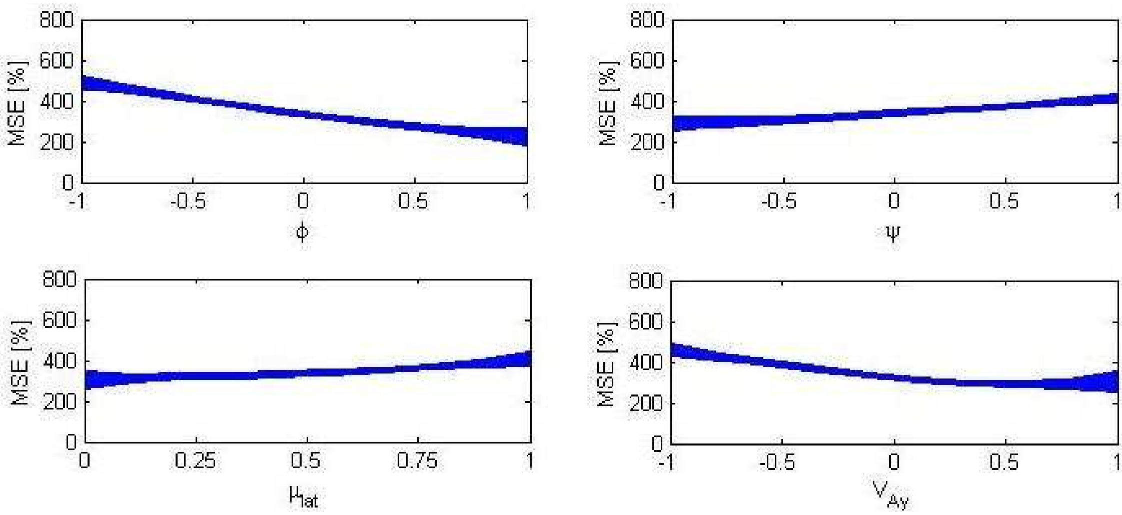

Fig. 12 Asymmetric Port MLG Spin Up Drag Axle Response Load Main Effects Plots

2. Aircraft Longitudinal Velocity

As V_{A_x} increases, the time required for spin-up, the maximum drag ground-to-load and the vertical ground-to tire-load increases [27]. While V_{A_x} is an input to the 'Actual' Landing model, ground speed is output by the Sensor and Data Acquisition System model and is typically used in a Hard Landing Analysis Process model. Ground speed is the resultant magnitude of the velocity component parallel to the earth's surface and therefore it is a function of the longitudinal and lateral velocities. While in symmetric landings, the ground speed is only a function of V_{A_x} since there is no lateral velocity, in asymmetric landings, it is a function of V_{A_x} and V_{A_y}. In the Sensor and Data Acquisition System model, filtering and sampling contributes an error of the magnitude of less than 1 m/s. This is consistent with the fact that ground speed is generally assumed to be constant in landing simulations. The main effects plots for V_{A_x} show that as V_{A_x} increases, the difference between the 'actual' and 'simulated' loads and moments do not increase linearly. Section V C will show that the contribution to the MSE from V_{A_x} alone is low and V_{A_x} is only significant for spin-up and spring-back when its interactions with other flight parameters are considered.

3. Aircraft Vertical Descent Velocity

The relationship between the MSE and V_{A_z} is nonlinear and tends to increase and level off at high vertical descent velocities. Figure 13 illustrates the difference between the peak aircraft vertical acceleration ($VRTG$) in the 'actual' landing and the peak $VRTG$ from the Sensor and Data Acquisition System model. At higher vertical descent velocities (and hence higher vertical accelerations), the possibility increases that the peak vertical acceleration will be missed on the FDR, due to low sampling rates (8 Hz) in conjunction with greater peak amplitudes. Therefore, the 'simulated' loads will be more under predicted as vertical descent velocity increases and the difference between the 'actual' and 'simulated' loads will be greater. However, conservatism in other flight parameters, such as μ_{long}, ensure that the landing gear loads are conservative.

As discussed in Section II, V_{A_z} is an input flight parameter, however the aircraft vertical acceleration measured by the FDR model is matched in the current hard landing analysis process model by iterating V_{A_z}. In the FDR model, the vertical acceleration is sampled and filtered and therefore any loss of data will have a significant impact on the landing gear loads modelled in the current hard landing analysis process model. Therefore, the vertical acceleration is one of the most important parameters in reducing the MSE.

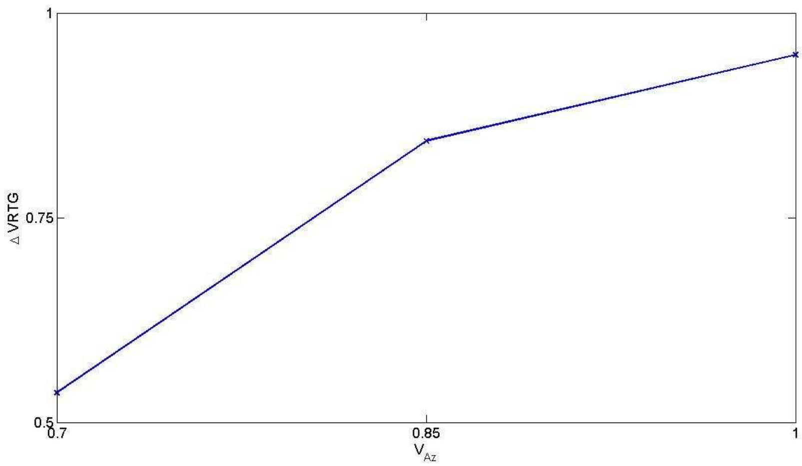

Fig. 13 Difference in Peak Aircraft Vertical Acceleration as a Function of Vertical Descent Velocity due to 8Hz Sampling Rate

4. Longitudinal & Lateral Tire-Runway Friction Coefficient

Figure 10 illustrates the relationship between MSE and μ_{long} for spin-up and spring-back drag axle response load bending moment. As the actual μ_{long} for the landing approaches the value assumed within the hard landing analysis process, the difference between the 'actual' and 'simulated' loads is reduced. This is logical considering that if the 'actual' landing has a tire-friction coefficient that is significantly lower than that assumed in the hard landing analysis process model, this will greatly contribute to the MSE.

There is a constant relationship between MSE and μ_{long} for vertical axle response load at maximum vertical reaction. In Section V C it is also shown that μ_{long} has little contribution to the vertical axle response load MSE.

The tire-runway interface is represented by a global friction potential delineated approximately by a circle, and the drag and side loads share the potential available in the tire-runway interface [28]. Therefore, in the case of combined slip in asymmetric landings, the drag and side ground-to-tire load depend on μ_{long} as well as μ_{lat}. As μ_{long} and μ_{lat} increase (the radius of the 'circle' increases), the drag load and side ground-to-tire load increase.

Due to the bookcase modelling technique that is used in the Hard Landing Analysis Process model and the relationship between the drag and side load and μ_{lat}, the drag axle response load and bending moment main effects plots show that MSE tends to increase as μ_{lat} increases. The MSE has a constant relationship with μ_{lat} for the maximum vertical reaction vertical axle response load MSE.

The MEI and TEI in Section V C show that μ_{long} is a very significant flight parameter. In its own right, μ_{lat} only tends to be significant when its interactions with other flight parameters are considered.

5. Main Landing Gear Shock Absorber Servicing State

In all of the main effects plots, the MLG shock absorber servicing state has a constant relationship with MSE. Therefore, the MSE is not sensitive to the shock absorber servicing state over its range and any shock absorber servicing state will give similar MSE values.

In the case of a symmetric landing, where the port and starboard MLG have the same servicing states, when the shock absorber is overinflated, higher loads are transmitted through the landing gear structure. However, because the shock absorber is stiffer (stiffer spring curve), there is a higher aircraft vertical acceleration for the same vertical descent velocity. In the hard landing analysis process model used in this study, the peak vertical aircraft acceleration is matched by iterating V_{A_z}. Therefore, if the correctly serviced shock absorber is used in the hard landing analysis process model while in the 'actual' case it is overinflated, a higher V_{A_z} will be required to match the vertical acceleration. Due to the fact that the vertical acceleration is being matched, the difference between the vertical and drag axle response loads and the bending moment from the landing with an overinflated shock absorber and from the landing with a correctly serviced shock absorber will be very similar.

When the shock absorber is underinflated, lower loads are transmitted through the landing gear structure and there is a lower aircraft vertical acceleration for the same vertical descent velocity. Therefore, if a correctly serviced shock absorber is assumed, meanwhile in the 'actual' case it is underinflated, the aircraft vertical acceleration will be higher and the loads in the 'simulated' landing will be higher and therefore, more conservative.

In the asymmetric landings, the port and starboard MLG shock absorber servicing states were altered independently and the analysis process did not correct for the mis-serviced shock absorber. However, the main effects plots show that the MSE is constant over the range of the port and starboard MLG servicing states, and the MEI and TEI, discussed in Section V C, indicate that the shock absorber servicing state is not significant. If another hard landing analysis process was introduced, that did not match the aircraft vertical acceleration, then an accurate assessment of the shock absorber servicing state may be more important.

6. Main Landing Gear Tire Pressure

In all of the symmetric and asymmetric main effects plots, the MLG tire pressure has a constant relationship with MSE. This indicates that the MSE is not sensitive to tire pressure over its range and any value of the tire pressure will give similar output values. Therefore, knowing the tire pressure is not useful in reducing the MSE.

7. Aircraft Mass & Centre of Gravity

For symmetric and asymmetric landings, the main effects plots for drag axle response load and bending moment at spin-up and spring-back show that the MSE is generally constant over the range of *mass* and the *CG*. However, the main effects plots for the maximum vertical reaction vertical axle response load MSE shows a non-linear relationship with *mass* and *CG*. As expected, as the *mass* and *CG* in the 'actual' landing moves further from the *mass* and *CG* in the 'simulated' landing, the MSE increases. This trend is more prevalent in the main effects plots for the vertical axle response load MSE than for spin-up and spring-back drag and bending moment MSE and is expected since the MEI and TEI, presented in Section V C, indicate that *mass* and *CG* are very significant to the vertical axle response load.

8. Aircraft Lateral Velocity

The main effects plots show that the difference between the 'actual' and 'simulated' loads increases on the starboard MLG as V_{A_y} increases. As described in Section II, in landings with with V_{A_y} that acts in the starboard direction, the MLG wheels touchdown at the same time and the starboard MLG has a higher vertical ground-to-tire load than the port MLG. As the initial aircraft lateral velocity and therefore lateral acceleration increases, the magnitude of the vertical ground-to-tire load increases on the starboard MLG, and decreases on the port MLG. However, the drag ground-to-tire load and axle response loads do not significantly change as the lateral velocity increases. In the Hard Landing Analysis Process model, described in Section III, the 'simulated' starboard vertical and drag loads were calculated using a bookcase method and the vertical and drag loads are factored up as a function of the LATG. Therefore, the 'simulated' drag load is being conservatively overestimated in the Hard Landing Analysis Process model. The same trend is seen with the bending moment MSE and vertical load MSE. These results are mirrored for the port MLG, as illustrated in Figure 12.

9. Aircraft Roll Angle

In a landing configuration with the aircraft rolled with the port wing down (negative roll angle), the aircraft first lands on the port MLG and then on the starboard MLG, as illustrated in Section II.

As the initial aircraft roll angle increases, the time between the wheels touching down increases and the build up of energy in the spin-up and spring-back is reduced. However, the spin-up and spring-back drag axle response load and bending moment main effects plots show that as the negative roll angle increases, the MSE increases. This is because the 'simulated' drag load at spin-up and spring-back is being conservatively overestimated in the Hard Landing Analysis Process model. The same effect occurs on the starboard MLG if there is a positive roll angle.

10. Aircraft Yaw Angle

The main effects plot for spin-up and spring-back drag axle response load and bending moment indicate that for the port MLG, the MSE increases as the positive yaw angle increases. As described in Section II, as the initial aircraft yaw angle increases, the port MLG spin-up and spring back loads decrease. Therefore, the 'simulated' port MLG spin-up and spring-back loads are being conservatively overestimated in the Hard Landing Analysis Process model.

C. Main Effects Indices and Total Effects Indices

Table 4 provides the MEI and TEI for the asymmetric landing sensitivity analysis. For brevity, only the asymmetric landing sensitivity study are given in tabular form, however the symmetric landing sensitivity analysis results are discussed with the asymmetric landing sensitivity analysis results. Input flight parameters with an MEI and TEI values above 10% are bold.

1. Spin-Up

a. Drag Axle Response Load: For both the symmetric and asymmetric landings, the MEI illustrate that μ_{long} and V_{A_z} contribute the most significantly to the spin-up drag axle response load MSE. The symmetric landing TEI show that along with μ_{long} and V_{A_z}, V_{A_x} and θ with their interactions, contribute to the spin-up drag axle response load MSE. For asymmetric landings, ϕ is also significant and V_{A_y} is as important as V_{A_x}. The asymmetric landing TEI show that θ, ψ and μ_{lat} and their interactions contribute to the drag axle response load MSE. The symmetric landing first order interactions account for 19.8% of the MSE. The interactions between μ_{long}-V_{A_z} (11.38%), μ_{long}-θ (1.73%), μ_{long}-V_{A_x} (1.68%) and V_{A_z}-V_{A_x} (1.87%) account for approximately 17%

Flight Parameter	Drag Axle Response Load				Bending Moment				Vertical Axle Response Load	
	Spin-Up		Spring-Back		Spin-Up		Spring-Back		Maximum Vertical Reaction	
	MEI [%]	TEI [%]	MEI [%]	TEI [%]	MEI [%]	TEI [%]	MEI [%]	TEI [%]	MEI [%]	TEI [%]
θ	1.47	5.47	2.92	**17.88**	1.46	5.77	7.75	**28.26**	0.93	**19.33**
V_{A_x}	3.41	9.08	7.21	**22.08**	0.59	2.84	0.50	0.50	0.16	1.25
V_{A_z}	8.60	**23.40**	1.17	**19.57**	7.24	17.97	0.13	6.70	**10.32**	**52.00**
μ_{long}	**45.93**	**61.37**	**39.16**	**68.56**	**18.27**	**29.98**	6.22	**14.95**	0.30	5.63
Port SA	0.06	1.23	0.05	0.06	0.10	0.26	0.06	2.12	0.15	0.30
Starboard SA	0.01	0.30	0.14	2.13	0.05	0.23	0.36	5.24	0.03	0.62
mass	0.12	1.13	0.09	2.98	1.64	13.56	2.52	**14.11**	8.91	**61.37**
CG	2.15	3.42	0.11	2.93	0.93	2.79	0.08	1.59	0.98	**26.94**
V_{A_y}	2.77	9.86	0.97	7.75	8.37	**39.92**	0.67	**42.36**	2.07	**11.56**
ϕ	6.09	**12.26**	2.78	**15.46**	5.35	**24.33**	9.40	**56.74**	0.94	**24.48**
ψ	1.36	4.28	1.27	6.21	3.07	**20.26**	0.69	**24.33**	0.48	1.83
μ_{lat}	0.82	5.81	2.00	8.39	3.12	**19.79**	2.21	**18.43**	0.22	2.36
First order interactions	18.84		19.99		27.84		36.12		48.66	
Higher order interactions	8.36		22.13		21.98		33.29		25.85	

Table 4 Asymmetric Port Main Landing Gear MSE MEI and TEI Summarized Results

of the MSE. The asymmetric landing first order interactions account for approximately 19% of the MSE. The greatest interactions are between μ_{long}-$V^e_{A_z}$ (7.27%), μ_{long}-ϕ (1.00%), V_{A_z}-V_{A_x} (1.94%) and V_{A_y}-μ_{lat} (1.06%) which account for approximately 11% of the MSE.

b. Bending Moment: The symmetric and asymmetric landing results are similar to the spin-up drag axle response load MSE: μ_{long} and V_{A_z} are the most significant parameters. However, V_{A_y} and ϕ are also very significant and the asymmetric landing TEI indicate that along with V_{A_y} and ϕ, ψ and μ_{lat} and their interactions contribute to the bending moment MSE. The asymmetric landing first order interactions account for approximately 27% of the MSE. The interactions between μ_{long}-V_{A_z} (3.00%), V_{A_y}-ϕ (4.57%), V_{A_y}-ψ (2.57%), V_{A_y}-μ_{lat} (3.62%), ϕ-ψ (1.36%) and ψ-μ_{lat} (1.06%) account for approximately 16% of the MSE.

c. Findings: In both the symmetric and asymmetric landings, the spin-up drag axle response load MSE and bending moment MSE may be reduced by learning the true value of μ_{long} and V_{A_z}. However, the asymmetric landings show that to reduce the drag axle response load MSE and bending moment MSE, it is also important to know the true value of V_{A_y} and ϕ, and that ψ and μ_{lat} have significant interactions with those parameters.

2. Spring-Back

a. Drag Axle Response Load: The symmetric and asymmetric landing MEI and TEI show similar results to the spin-up drag axle response load: μ_{long}, V_{A_z}, V_{A_x}, θ and ϕ are the most significant parameters, while V_{A_y}, ψ and μ_{lat} are also important parameters. However, the TEI also shows that *tire* and its interactions have an effect on the the spring-back drag axle response load MSE. The following first order interactions account for approximately 18% of the MSE in the symmetric landings: μ_{long}-V_{A_z} (9.14%), μ_{long}-V_{A_x} (2.94%), μ_{long}-θ (2.84%), μ_{long}-*tire* (2.0%) and V_{A_z}-*tire* (1.19%). In the asymmetric landings, first order interactions account for approximately 20% of the MSE. The following interactions account for approximately 10% of the MSE: μ_{long}-V_{A_z} (4.04%), μ_{long}-θ (3.54%), μ_{long}-V_{A_x} (2.15%). In the symmetric landing sensitivity study, *tire* was an important parameter and although it was not considered in the asymmetric landing sensitivity study, by similarity *tire* is also an important parameter for asymmetric landings. Therefore, μ_{long}, V_{A_z}, ϕ and *tire* are important parameters in the spring-back drag axle response load MSE.

b. Bending Moment: Like the spring-back drag axle response load MSE, μ_{long}, V_{A_z}, V_{A_x}, θ and *tire* contribute significantly to the spring-back bending moment MSE. In the symmetric landings, the following interactions account for approximately 23% of the MSE: μ_{long}-V_{A_z} (5.16%), μ_{long}-θ (13.31%), μ_{long}-*mass* (2.04%) and V_{A_x}-θ (2.34%). Therefore, *mass* is also a significant parameter for spring-back bending moment MSE. For asymmetric landings, ϕ is also important and the following first order interactions account for approximately 23% of the MSE: μ_{lat}-θ (2.88%),

V_{A_y}-ϕ (12.95%), θ-ϕ (2.27%), ϕ-ψ (3.78%) and ϕ-μ_{lat} (1.43%). Therefore μ_{long}, V_{A_z}, *tire*, *mass* and ϕ are the important parameters for the spring-back bending moment MSE.

c. Findings: In order to reduce the spring-back drag axle response load MSE and bending moment MSE, the true value of μ_{long}, V_{A_z}, ϕ, V_{A_y}, *mass* and *tire* must be learned.

3. Maximum Vertical Reaction

a. Vertical Axle Response Load: The symmetric and asymmetric landing MEI illustrate that *mass* and V_{A_z} contribute significantly to the vertical axle response load MSE. The symmetric landing TEI show that along with *mass* and $V^e_{A_z}$, *CG*, θ and *tire* with their interactions, contribute to the vertical axle response load MSE. The symmetric landing first order interactions account for approximately 49% of the MSE. The interactions between *mass*-V_{A_z} (15.38%), *mass*-*CG* (13.63%), *mass*-θ (4.10%), $V^e_{A_z}$-*CG* (4.02%), V_{A_z}-θ (2.32%), *mass*-*tire* (1.92%) account for approximately 41% of the MSE. The asymmetric landing TEI show that ϕ and its interactions also contributes to the vertical axle response load MSE. The asymmetric landing first order interactions also account for approximately 49% of the MSE. The interactions between V_{A_z}-θ (2.22%), V_{A_z}-*mass* (12.87%), V_{A_z}-ϕ (2.19%), θ-*mass* (3.49%), *mass*-*CG* (7.92%) and *mass*-ϕ (7.01%) account for approximately 36% of the MSE.

b. Findings: The maximum vertical reaction vertical axle response load MSE may be reduced by learning the true value of μ_{long}, V_{A_z}, ϕ, *mass*, *CG*. From the symmetric landing sensitivity study, it was also seen that *tire* was an important parameter to learn in order to reduce the MSE.

VI. Summary of Significant Flight Parameters

A summary of the significant flight parameters is presented in Table 5. Each parameter is rated as *High* (H), *Medium* (M) or *Low* (L). *High* identifies flight parameters that greatly influence the MSE, *Medium* identifies flight parameters that have some influence on the MSE and *Low* identifies flight parameters that have little or no influence on the MSE.

Flight Parameter	Significance (H/M/L)
ϕ	H
θ	M
ψ	H
V_{A_x}	M
V_{A_y} $(LATG)$	H
V_{A_z} $(VRTG)$	H
$mass$	M
CG	M
$tire$	M
$tire\ press$	L
$Port\ SA$	L
$Starboard\ SA$	L
μ_{long}	H
μ_{lat}	H

Table 5 Summary of the Significant Flight Parameters in Reducing the MSE

VII. Conclusions

The purpose of this paper was to investigate the sensitivity of input parameters varied in the FPSS model to the difference between the 'actual' and 'simulated' loads in symmetric and asymmetric, two-point landings, calculated as MSE. The sensitivity analysis provided the following conclusions:

- Longitudinal runway friction coefficient, aircraft vertical descent velocity, aicraft lateral velocity and aircraft roll angle contributed the most to the spin-up and spring back drag axle response load MSE and bending moment MSE.
- Aircraft vertical descent velocity, roll angle, mass, centre of gravity position and MLG tire type had significant influences on the maximum vertical reaction vertical axle response load MSE.
- While V_{A_x} and θ did not change considerably from the 'actual' to the 'simulated' landing, the

interactions with μ_{long} and V_{A_z} contributed to the MSE in all cases.

- The flight parameters ψ and μ_{lat} are only significant when their interactions are considered.

- Due to the Hard Landing Analysis Process modelling technique, $VRTG$ is as significant as V_{A_z}, and $LATG$ is as significant as V_{A_y}, in reducing MSE.

- It was also shown that over the range in this sensitivity study, and due to the modelling techniques used in the Hard Landing Analysis Process model used in this study, the shock absorber servicing state and MLG tire pressure do not contribute significantly to the MSE and learning the true value of these flight parameters would not reduce the MSE.

For symmetric and asymmetric two-point landings, the MSE can be reduced by learning the true value of the following flight parameters: μ_{long}, $VRTG$ (related to V_{A_z}), $LATG$ (related to V_{A_y}), ϕ, ψ, $mass$, CG and $tire$.

Acknowledgments

The authors would like to thank the following colleagues at Messier-Bugatti-Dowty for their invaluable assistance in the model development and sensitivity study analysis: Laura Collett, Sidney Smith and Andrew Thomas.

The authors would also like to thank Dr. Marc Kennedy of the Probability and Statistics Department at the University of Sheffield for the use of GEM-SA.

This paper would not have been possible without the financial support of Messier-Bugatti-Dowty and the Knowledge Transfer Partnerships (KTP) program through partnership number 1216. This KTP was funded by the Technology Strategy Board.

References

[1] "Certification Specifications for Large Aeroplanes, CS25," European Aviation Safety Agency, 2008.

[2] "Airworthiness Standards: Transport Category Airplanes, FAR 25," , 2008.

[3] Schmidt, R. K. and Sartor, P., "Landing Gear," in Boller, C., Chang, F.-K., and Fujino, Y., eds., "Encyclopaedia of Structural Health Monitoring," Wiley, 2009, pp. 1983–1994.

[4] Sartor, P., Bond, D., Staszewski, W., and Schmidt, R. K., "Assessment of the Value of an Overload Indication System through Analysis of Aviation Industry Occurrence Data," *AIAA Journal of Aircraft*, Vol. 46, No. 5, 2009, pp. 1692–1705.

[5] Sartor, P., Schmidt, R. K., Menezes, R., Bond, D., and Staszewski, W., "Validation and Verification of a Hard Landing Indication System for Aircraft Landing Gear," in "Proceedings of 7th International Workshop on Structural Health Monitoring," Stanford, U.S.A., 2009, pp. 190–200.

[6] Saltelli, A., Chan, K., and Scott, E. M., *Sensitivity Analysis*, Wiley, 2000.

[7] Oakley, J. E. and O'Hagen, A., "Probabilistic Sensitivity Analysis of Complex Models: A Bayesian Approach," *Journal of the Royal Statistical Society Series B*, Vol. 66, No. 3, 2004, pp. 751–769.

[8] Worden, K. and Manson, G., "On the Identification of Hysteretic Systems, Part I: Fitness Landscapes and Evolutionary Identification," *Mechanical Systems and Signal Processing*, Vol. 29, 2012, pp. 201–212.

[9] Wright, J. R. and Cooper, J. E., *Introduction to Aircraft Aeroelasticity and Loads*, Wiley, 2007.

[10] Currey, N. S., *Aircraft Landing Gear Design: Principles and Practices*, American Institute of Aeronautics and Astronautics, Washington, D.C., 1988.

[11] Milwitzky, B., Lindquist, D., and Potter, D., "An Experimental Study of Applied Ground Loads in Landing," Tech. Rep. 1248, NACA, 1955.

[12] Lomax, T. L., *Structural Loads Analysis for Commercial Transport Aircraft: Theory and Practice*, AIAA Education Series, 1996.

[13] Becker, W., J. Rowson, J., Oakley, J., Yoxall, A., Manson, G., and Worden, K., "Bayesian Sensitivity Analysis of a Model of the Aortic Valve," *Journal of Biomechanics*, Vol. 44, 2011, pp. 1499–1506.

[14] Kennedy, M. C. and O'Hagen, A., "Bayesian Calibration of Computer Models," *Journal of the Royal Statistical Society: Series B (Statistical Methodology)*, Vol. 63, No. 3, 2001, pp. 425–464.

[15] Kennedy, M. C., Anderson, C. W., Conti, S., and O'Hagen, A., "Case Studies in Gaussian Process Modelling of Computer Codes," *Reliability Engineering and System Safety*, Vol. 91, No.10-11, 2006, pp. 1301–1309.

[16] Sacks, J., Welch, W. J., Mitchell, T. J., and Wynn, H. P., "Design and Analysis of Computer Experiments," *Statistical Science*, Vol. 4, No. 4, 1989, pp. 409–435.

[17] Rasmussen, C. E. and Williams, C. K., *Gaussian Processes for Machine Learning*, The MIT Press, 2005.

[18] Sobol, I., "Sensitivity Estimates for Non Linear Mathematical Models," *Mathematical Modeling Computer Experiment*, Vol. 1, 1993, pp. 407–414.

[19] Petropoulos, M., G. anf Wooster, Carlson, T., Kennedy, M. C., and Scholze, M., "A Global Bayesian Sensitivity Analysis of the 1d SimSphere Soil-Vegitation-Atmospheric Transfer (SVAT) Model Using Gaussian Model Emulation," *Ecological Modelling*, Vol. 220, 2009, pp. 2427–2440.

[20] Homma, T. and Saltelli, A., "Importance Measures in Global SensitivityAnalysis of Nonlinear Models," *Reliabillity Engineering & System Safety*, Vol. 52, No. 1, 1996, pp. 1–17.

[21] Kennedy, M. C., "GEM-SA Homepage," http://ctcd.group.shef.ac.uk/gem.html.

[22] Le Gratiet, L., Cannamela, C., and Iooss, B., "A Bayesian Approach for Global Sensitivity Analysis of (Multifedilty) Computer Codes," *SIAM/ASA Journal of Uncertainty Quantification*, Vol. 2, 2014, pp. 336–363.

[23] Gramacy, R. B. and Taddy, M., "Categorical Inputs, Sensitivity Analysis, Optimization and Importance Tempering with tgp Version 2, an R Package for Treed Gaussian Process Models," *Journal of Statistical Software*, Vol. 33, No. 6.

[24] Becker, W., Worden, K., and Rowson, J., "Bayesian Sensitivity Analysis of Bifurcating Nonlinear Models," *Mechanical Systems and Signal Processing*, Vol. 34, No. 1-2, 2013, pp. 57–75.

[25] Worden, K. and Becker, W., "On the Identification of Hysteretic Systems, Part II: Bayesian Sensitivity Analysis and Parameter Confidence," *Mechanical Systems and Signal Processing*, Vol. 29, 2012, pp. 213–227.

[26] Bayarri, M., Berger, J., Higdon, D., Kennedy, M., Kottas, A., Paulo, R., Sacks, J., Cafeo, J., Cavendish, J., Lin, C., and Tu, J., "A Framework for Validation of Computer Models," Tech. rep., National Institute of Statistical Sciences, General Motors, 2002.

[27] Milwitzky, B., Lindquist, D., and Potter, D., "An Experimental Study of Wheel Spin-Up Drag Loads," Tech. Rep. 3246, NACA, 1954.

[28] "The Tyre Grip," Tech. rep., Michelin.